Probing the tail of the nuclear potential between identical nuclei with quasi-elastic Mott scattering

著者	Hinde D. J., Ahlefeldt R. L., Thomas R. G., Hagino K., Brown M. L., Dasgupta M., Evers M., Gasques L. R., Rodriguez M. D.
journal or publication title	Physical Review. C
volume	76
number	1
page range	014617
year	2007
URL	http://hdl.handle.net/10097/52590

doi: 10.1103/PhysRevC.76.014617

Probing the tail of the nuclear potential between identical nuclei with quasi-elastic Mott scattering

D. J. Hinde, R. L. Ahlefeldt, R. G. Thomas, K. Hagino,* M. L. Brown, M. Dasgupta, M. Evers, L. R. Gasques, and M. D. Rodriguez

Department of Nuclear Physics, Research School of Physical Sciences and Engineering, Australian National University, Canberra, ACT 0200, Australia

(Received 10 May 2007; published 27 July 2007)

Elastic scattering of identical nuclei results in oscillatory Mott scattering. The separation of the peaks is perturbed by the presence of the nuclear potential. Near-barrier measurements of Mott scattering of ^{58}Ni from ^{58}Ni have been made to obtain information on the diffuseness of the nuclear potential, giving a diffuseness parameter of 0.62±0.04 fm.

DOI: 10.1103/PhysRevC.76.014617 PACS number(s): 24.10.Eq, 25.70.Bc

I. INTRODUCTION

Measurements of fusion of nickel isotopes have played a major role in demonstrating the effects on fusion cross sections of neutron transfer [1], multiple quadrupole phonon couplings [2], and suppression of deep-subbarrier fusion [3]. The nuclear potential plays a crucial role in calculations aiming to quantitatively interpret these experimental observations. For the commonly used Woods-Saxon nuclear potential, the diffuseness parameter determines the tail of the potential, which is relevant to both fusion and scattering processes. The diffuseness is expected to be in the range ∼0.6–0.7 fm, both from theoretical approaches, for example, double-folding model calculations [4] of the nuclear potential, and from global analyses of scattering data. However, a systematic study [5] of many high precision experimental above-barrier fusion excitation functions has shown that there is a systematic deficit in measured fusion cross sections compared with calculations using a Woods-Saxon nuclear potential with such standard values of diffuseness. The data can be well reproduced within a barrier passing (coupled-channels) picture using nuclear diffuseness parameters systematically larger than (up to twice) those expected. It is crucial to determine whether this discrepancy should be attributed to an unexpected behavior of the nuclear potential or to other physical processes not included in a potential picture.

In the reactions of Ni isotopes, these systematics [5] predict that a diffuseness of 1.1 fm should be required to reproduce the above-barrier fusion excitation functions. The significant structures found in the first measured barrier distribution for nickel isotopes (for ^{58}Ni+^{60}Ni [2]) were reproduced with coupled-channels calculations, including multiple-phonon couplings, using a diffuseness of 0.90 fm. Within a coupled-channels framework, the diffuseness of the nuclear potential determines the barrier width and the nuclear coupling strengths, thus it is an important input to the calculations. Recently, this barrier distribution has been remeasured [6], and preliminary analysis suggests additional couplings are needed compared with those of Ref. [2]. However, final interpretation and conclusions will need further coupled-channels calculations. New information on the appropriate nuclear potential to use in the calculations is thus of current importance. It will also help in understanding the systematic observation of fusion cross sections smaller than predicted using standard diffuseness values, for both deep-subbarrier and above-barrier energies.

It has recently been shown [7,8] that subbarrier quasi-elastic scattering at backward angles is sensitive to the tail of the nuclear potential but can be insensitive to coupling effects [9], making the approach attractive for determining unambiguously the outer region of the nuclear potential. Measurements [9] of quasi-elastic scattering of ^{32}S from a range of heavy targets (carried out specifically for such an analysis) have shown that it is possible to obtain quite precise information on the potential through high quality measurements. In collisions of similar mass nuclei, such as the collisions of nickel isotopes, this technique is experimentally more difficult, as recoiling target nuclei are present in large numbers at angles where the backward-recoiling projectile nuclei need to be measured.

However, in the case of collisions of identical nuclei, the situation is quite different. As expected, and experimentally observed [10], because of the quantum-mechanical requirement of symmetrization or antisymmetrization of the wave function under interchange of bosons or fermions, scattering of identical nuclei results in Mott scattering rather than Rutherford scattering. Mott scattering has an angular distribution symmetric about 90° in the center-of-mass (c.m.) frame, with pronounced oscillations due to interference between the forward and backward amplitudes. In the limit of a point Coulomb interaction, an expression for Mott scattering, and thus the separation of the oscillations, can be written analytically [11]. The results of such a calculation are shown in Fig. 1 for the scattering of ^{58}Ni + ^{58}Ni at a center-of-mass energy $E_{\mathrm{c.m.}} = 80$ MeV.

It is important to note that the angular separation of the oscillations is sensitive to departures from a point Coulomb potential. The largest deviation from a point Coulomb potential results from the tail of the nuclear potential. Thus measurement of Mott scattering may be a sensitive probe of the nuclear potential, analogous to counting light fringes to determine small changes in distance.

*Current address: Department of Physics, Tohoku University, Sendai 980-8578, Japan.

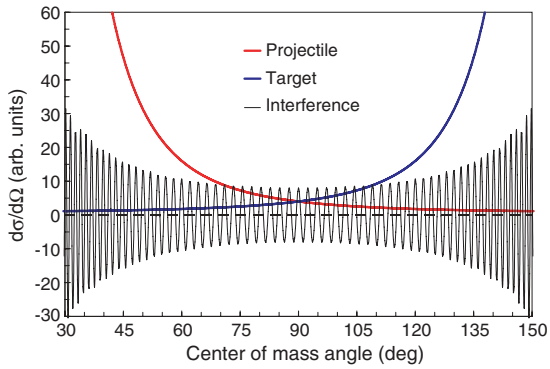

FIG. 1. (Color online) Three components making up Mott scattering, as calculated with the analytical point Coulomb Mott scattering expression. Although the oscillating interference component increases in amplitude away from 90°, the projectile and target nucleus components increase more rapidly, as $1/\sin^4(\theta/2)$ and $1/\cos^4(\theta/2)$, thus the Mott oscillations are seen most clearly around 90°.

In the case of ^{58}Ni + ^{58}Ni at energies near the fusion barrier, the Mott scattering peaks are separated by 1.2° to 1.4° in the laboratory frame. The peaks are most pronounced around 45°, thus an experiment was carried out to make measurements symmetrically around this angle. Measurements were made at and below the fusion barrier energy and at an energy 10% above the fusion barrier.

II. EXPERIMENTAL PROCEDURE

Beams of ^{58}Ni at energies $E_{\rm lab}$ of 160, 190, 200 and 220 MeV were provided by the Australian National University's 14 UD tandem electrostatic accelerator. They bombarded an enriched self-supporting target of 50μg/cm^2 ^{58}Ni, oriented normal to the beam. The (small) energy loss of the beam to the midpoint of the target was taken into account in the calculations described later. The beam was focused through a 2 mm diameter aperture on the target ladder for each beam energy to obtain a consistent beam-spot position. From the nearly full transmission through the aperture, the full width at half maximum (FWHM) of the beam spot was determined to be $\leqslant$1 mm. Scattered particles were detected in two large position sensitive multiwire proportional counters (MWPCs) with active areas 284 by 357 mm, located on either side of the beam axis. The normal to the detector center electrodes, at a scattering angle of 45°, was 222.4 mm from the target, resulting in a minimum period of the Mott oscillations on the detector of ∼5 mm. Despite the wire spacing being 1 mm, the generation of signals on two adjacent wires for those particles not passing close to only a single wire results in a position resolution somewhat better than 1 mm and thus smaller than the typical beam-spot size. Although the detectors covered a scattering angle range of 7° to 70°, angles less than ∼30° and greater than ∼60° were blocked to ensure the measurement of the most prominent oscillations (around 45°) were not limited by the high count rate at more forward and backward angles. With an azimuthal acceptance angle for coincidence events of ∼90°, several million Mott scattering events were collected

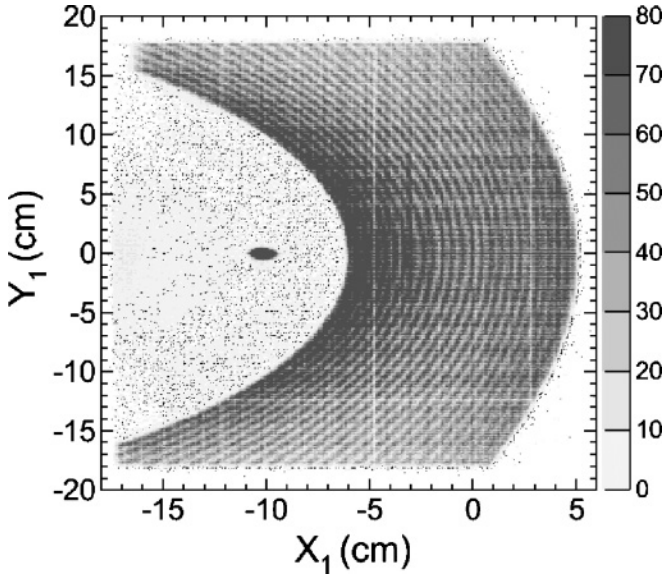

FIG. 2. Matrix of calibrated X vs Y positions, for detector 1, for the measurement at 160 MeV. The grey scale on the right indicates the number of counts per pixel. The Mott oscillations (curved lines) and the shadows of 0.45 mm diameter window support wires (straight lines at, e.g., $X = -4.8$ cm) are clearly visible.

in ∼30 min at each energy. The signals recorded, triggered by an event in either detector, were the X and Y position and the energy loss signals in each detector, together with the time signals from the detector center foils. Because energy was not determined directly but could only be inferred with several MeV uncertainty from the angular information from the two detectors, the measurement comprised the sum of elastic and inelastic scattering, termed quasi-elastic scattering. Since essentially all observed events corresponded to the desired ^{58}Ni + ^{58}Ni scattering, the most significant parameters were X and Y, from which the Mott oscillation characteristics can be determined. Figure 2 shows the X vs Y matrix for one of the detectors, at 160 MeV, without the requirement of a coincident particle in the other detector. The mask blocking the angles forward of ∼30° had an aperture in it, seen at $X = -10$ cm, $Y = 0$ cm. Gas window support wires of 0.45 mm diameter, whose projections were located at $X = 2.9, -4.8$, and -12.2 cm, and $Y = -4.2$ and $+4.2$ cm, and -12.5 and $+12.5$ cm, block the scattered particles. The Mott oscillations are very clearly visible.

III. DETECTOR CALIBRATION

Since the aim of the experiment was to measure small deviations in the period of the Mott oscillations due to the nuclear potential, detector angle calibration was a critical ingredient of the experimental analysis.

A. Angle calibration

The first step in angle calibration was absolute position calibration of events within the detectors. The position calibration

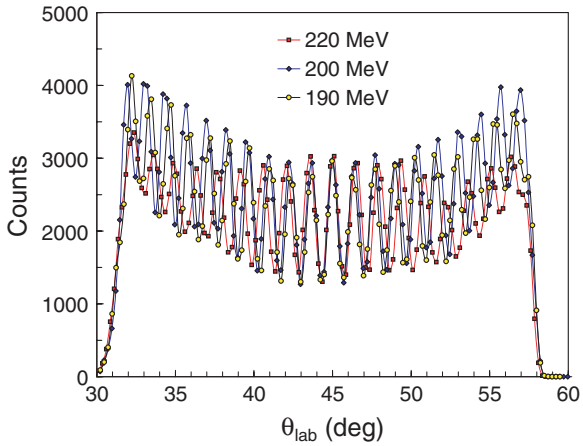

FIG. 3. (Color online) Counts as a function of laboratory angle for three beam energies, showing that the angle of the 45° peak alone is independent of energy, as expected if the angle calibration is correct.

of the X and Y spectra used the detector edges and the known detector sizes to generate the spectrum shown in Fig. 2. This calibration was found to be consistent at all energies. Using the position information from the MWPCs, and the target-detector geometry, in the event-by-event analysis the X and Y position information was converted to scattering angle θ and azimuthal angle ϕ. This initial detector angle calibration was carried out using the designed geometry of the target and detectors; however, because of the large size of the detectors, it was anticipated that deviations of as much as ∼1 mm could occur. The position of the Mott oscillation at 45° in the laboratory frame (90° in the c.m. frame) does not vary with energy, and this was used to confirm that there was no significant error in the initial calibration. The angular distributions determined at a number of energies are shown in Fig. 3, demonstrating that this peak has been correctly identified, showing no shift with energy. The angular distribution at 160 MeV, which is at only 80% of the fusion barrier energy, was measured specifically to allow exact detector angle calibration. This is possible because the angles of the Mott oscillation peaks at this low energy are essentially independent of the nuclear potential parameters.

In addition to the nuclear potential, and couplings to excited states (discussed below), a number of small effects cause Mott scattering to deviate slightly from the form expected from a point Coulomb potential. These are relativistic effects, nuclear polarizability, electron screening, and vacuum polarization. These effects were calculated in Ref. [12] for the Mott scattering of ^{208}Pb + ^{208}Pb. It was there found that the summed angular shift of the Mott oscillations at 30° was 0.05°. More significantly, over a 20% beam energy range, the calculated angular shift changed by only 0.02°. This is far smaller than the precision required in this work to obtain information on the nuclear potential, and we effectively incorporate these effects, in an energy-independent way, into the detector angular calibration by fine tuning the detector geometrical calibration to match the Mott scattering calculation at 160 MeV, and use this calibration for higher energies. A further effect that may become significant as the beam energy increases over the fusion barrier is the charge form factor of the nuclei. Along with the nuclear potential and couplings, this is treated explicitly in the calculations.

Fine tuning of the channel numbers corresponding to the edge and centers of the two detectors was carried out for the 160 MeV measurement to achieve three goals:

(i) The 45° peak should be exactly at 45°.
(ii) The peaks in θ should be independent of ϕ.
(iii) All the peaks should match the calculated Mott scattering angles.

Additional checks coming from the coincidence between the two detectors were that (i) the folding angle in the laboratory frame between elastically scattered pairs of nuclei should be 90° and (ii) the azimuthal angle between the two particles should be 180°.

Mott scattering was calculated using a specially modified version of the code CCFULL [13]. Initially, calculations with no couplings were used; however, it was found that even at 160 MeV, where the nuclear potential plays no role, Coulomb coupling has a small but significant effect on the period of the Mott oscillations. Different calculations were carried out with one, two, and three quadrupole phonons in each nucleus, including all mutual excitations. It was found that the calculations were not sensitive to the number of phonons included. This will be illustrated later. The data at 160 MeV were matched to the calculations including two quadrupole phonons, as existing measured Ni+Ni fusion barrier distributions can only be reproduced with two or more phonons in each nucleus.

The resulting θ vs ϕ matrix for coincident events at 160 MeV is shown in Fig. 4, for one of the detectors, calibrated to give the best achievable match to the above criteria. The

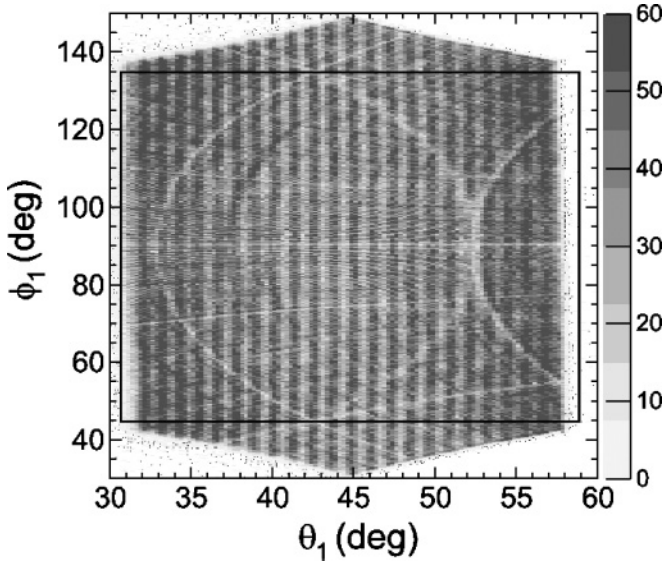

FIG. 4. Matrix of events in detector 1 in coincidence with detector 2, as a function of laboratory scattering angle θ and azimuthal angle ϕ, for the 160 MeV calibration reaction. The Mott oscillations, independent of ϕ, are clearly seen. The black rectangle represents the gate used to determine $d\sigma/d\theta$. Detailed features of the spectrum are discussed in the text.

Mott oscillations are very clear, independent of ϕ. The pale curved lines (corresponding to low intensity) which increase in θ as ϕ deviates from 90° are due to blocking by the window support wires of this detector; those with the opposite curvature result from blocking of events due to the support wires of the complementary detector, mapped onto this detector through the scattering kinematics. Other slight modulations (dark curves) result from small local nonlinearity in the detector X and Y position response. Detector 1, whose response is shown in the figure, had slightly the better linearity of the two, so it was the one used for the subsequent Mott oscillation angle analysis. The rectangular box shown in Fig. 4 represents the gate applied to obtain the angular distributions, having an azimuthal angle acceptance of 90°, independent of θ.

The measured angular distributions in the laboratory frame shown in Fig. 3 (and later in Fig. 6) are proportional to $d\sigma/d\theta$ rather than $d\sigma/d\Omega$, since the azimuthal acceptance is angle independent. Conversion of the Mott calculations (made in the c.m. frame) to the laboratory frame requires multiplication of the calculations by $2\pi \sin\theta$ (to obtain $d\sigma/d\theta$ from $d\sigma/d\Omega$) as well as by the solid angle factor of $4\cos\theta$ in converting to the laboratory reference frame. The product $\sin\theta\cos\theta$ is symmetric about 45° in the laboratory frame. Thus the measured raw $d\sigma/d\theta$ spectrum should also be symmetric about 45° in the laboratory frame, since the Mott scattering is symmetric about 90° in the c.m. frame. This symmetry is made use of in Sec. III C. The same considerations apply in the later conversion of the experimental data to the c.m. frame.

After the angle calibration, the folding angle in both azimuthal and scattering angle matched expectations very well. The scattering angle in one detector vs that in the other is shown in Fig. 5 for the 160 MeV calibration measurement. The Mott oscillations lie on a diagonal summing to 90°, indicated by the thin diagonal line. At somewhat larger angles, a small parallel ridge is present, peaking at slightly more than 46° in both detectors. This is consistent with scattering of the ^{58}Ni from copper, the expected angles for scattered ^{58}Ni and recoiling ^{63}Cu being indicated by the thin intersecting lines. The nickel foil was initially evaporated onto a copper substrate, which was subsequently etched away. A very small amount of copper must have remained. This has no effect on the determination of the positions of the Mott scattering peaks for ^{58}Ni + ^{58}Ni, as the yield is small and smoothly varying with angle.

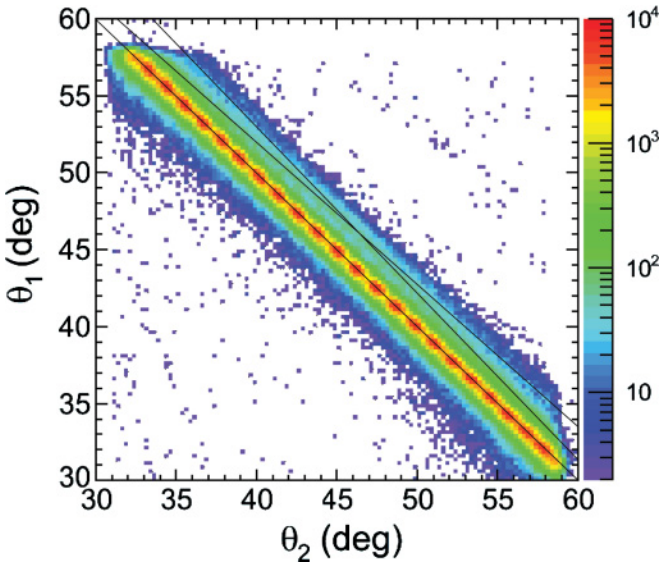

FIG. 5. (Color online) Matrix of events as a function of laboratory angle θ measured in detectors 1 and 2, for the 160 MeV calibration reaction. The color scale on the right indicates the counts per pixel. The Mott peaks lie on the diagonal line with folding angle 90°. The expectations for scattered Ni and recoiling Cu nuclei resulting from scattering from a copper impurity in the target are indicated by the intersecting lines (see text).

B. Angular resolution

In determining how the nuclear potential diffuseness should best be extracted from the experimental data, it proved valuable to understand the sources of loss of angular resolution in the experiment. The experimental angular resolution is expected to have a considerable number of contributions. Detector position resolution of better than 1 mm contributes ∼0.2° FWHM. The beam-spot size, ∼1 mm FWHM, seen by the detectors at a typical angle of 45°, also contributes ∼0.2°. Detector nonlinearity is estimated to contribute 1 mm FWHM (0.25°). The contribution from beam divergence at the target can range from less than 0.1° to a maximum of 0.4°, depending on the settings of beam-limiting irises. Finally, multiple scattering in the target is calculated to make the largest single contribution of 0.5° FWHM at 45°, decreasing at smaller detector angles, and increasing at larger angles. Adding all these effects in quadrature gives a typical expected FWHM between 0.63° and 0.74°. If the target were infinitely thin, this would reduce to between 0.38° and 0.55°. However, the resolution with the 50μg/cm^2 target that was used was more than adequate to characterize the Mott oscillations. There is a complicated geometrical relationship between the resolution and position on the detector, which can only be estimated, as discussed above. To determine the approximate validity of the above estimates, a simple approach to determining the average experimental angular resolution was taken. The calculated Mott scattering for 160 MeV was fitted to the measurement by convoluting it with a single Gaussian function whose width was varied to obtain the minimum χ^2. The FWHM obtained was 0.68°, consistent with the 0.63° to 0.74° range estimated above. The same width was also found for other beam energies.

Figure 6 shows the experimental angular distribution for 160 MeV on an expanded angular scale, together with the raw Mott scattering calculation, and the calculation convoluted with the best-fitting Gaussian function. Close inspection of the deviations between the data and the fit show that the resolution must indeed have a systematic variation with angle, in a manner consistent with the sources of angular spreading discussed above. The resolution is better forward of 45° and worse at more backward angles, where the effect of multiple-scattering, the largest contribution, increases. The χ^2 of the fit is poor, being dominated by the angle-dependent experimental resolution. For this reason, and the uncertainties in calculating the actual angle dependence, it was considered

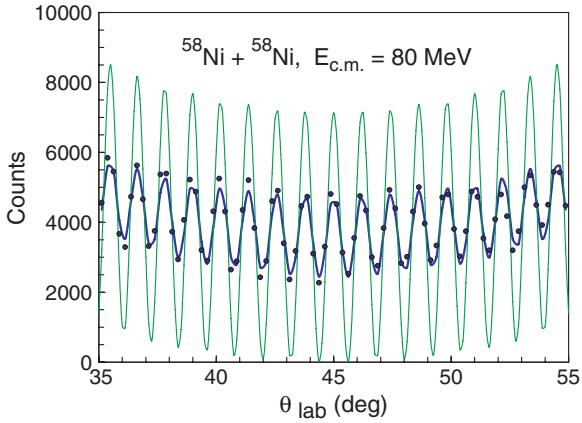

FIG. 6. (Color online) Experimental angular distribution proportional to $d\sigma/d\theta$ (points), and calculated Mott oscillations, as a function of laboratory angle. The thin curve shows the oscillations without folding the experimental angular resolution; the thick curve includes 0.68° FWHM experimental resolution. The comparison shows that the experimental resolution is θ dependent (see text).

that finding the best-fitting nuclear potential diffuseness should be carried out through a process involving fitting the individual peaks to determine their angles, rather than fitting the full angular distributions by calculations using different nuclear potentials. This process is described in Sec. IV.

C. Correction for beam characteristics

The measurement relies on a consistent geometrical configuration from run to run. The beam characteristics play a role in defining the geometry. Tuning of the beam onto the target was carried out with the aim of obtaining a consistent geometry for all beam energies. Since about 90% of the beam was focused through the circular 2 mm diameter beam tuning aperture, correct maximization should allow little possibility of substantial beam-spot shifts. However, there was the possibility that from energy to energy, the incident angle of the beam could shift slightly, as could the centroid of the beam spot, on a sub-mm scale. These possibilities could be checked, having detectors on both sides of the beam. The center of the Mott oscillation pattern could be accurately determined by matching the measured angular distributions around a "mirror angle" of $(45 + \delta)^\circ$, where δ is an angle offset adjusted to optimize the overlap. The mirror angles so determined in the two detectors are shown in Fig. 7 for each energy. The results from the two detectors are consistent with a physical change in the beam characteristics from run to run, as they shift by equal and opposite amounts. If the shifts were due solely to a position shift of the beam spot, for the detector whose angle is larger than 45°, the beam spot is closer, and the angular separation of the Mott peaks would be slightly too large. The converse would apply in the complementary detector. Experimentally, comparison of the angular separation of the Mott peaks in the two detectors showed no evidence for such a beam-spot movement with beam energy. Thus the angle changes of up to 0.09° are attributed to differences in the angle of the beam passing through the target. The peak

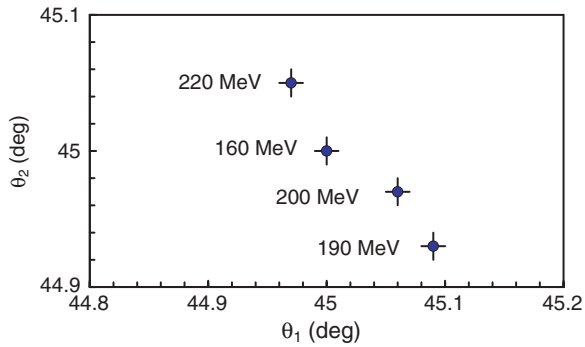

FIG. 7. (Color online) Laboratory-frame mirror angles of the measured angle spectra in the two detectors, representing the angles of the central peaks for each beam energy (see text). The points lie on a diagonal consistent with slight beam angle shifts from run to run (see text).

analysis procedure described below is independent of such angle changes, so no explicit angle correction was applied in the subsequent Mott oscillation analysis.

IV. DETERMINATION OF NUCLEAR POTENTIAL DIFFUSENESS

A. Approach

By determining the Mott oscillation peak angles from the experiment and comparing them with calculations, we investigated the tail of the nuclear potential. The effect of the nuclear potential is to shift the angle between Mott oscillation peaks by an approximately constant amount for each oscillation. Determining the cumulative angle shift over a considerable number of oscillations thus gives the greatest sensitivity. The positions of the Mott scattering peaks in the measurements were determined by fitting a polynomial background matching the locus of the minima between peaks, and fitting a Gaussian to each peak. To be consistent with this procedure, the peak positions in the calculations were obtained from the maxima in the ratio of the calculated Mott scattering cross section to the sum of the squares of the forward and backward amplitudes.

The measurements were compared with calculations performed with a modification of the quasi-elastic coupled-channels version of the code CCFULL [7], taking into account the special conditions of scattering of identical particles. A Woods-Saxon nuclear potential form was used in the calculations, with various values of the diffuseness parameter. The parameters of the Woods-Saxon potential were constrained by the fusion barrier energy, for which a value of 99.0 MeV was used. This was obtained in a preliminary analysis of a recently measured fusion excitation function for this reaction [6]. However, taking the nuclear potential used in the coupled-channels calculations for ^{58}Ni +^{60} Ni (99.8 MeV) quoted in Ref. [2], a barrier energy for the ^{58}Ni +^{58} Ni reaction of 100.3 MeV is obtained. Using the Akyuz-Winther potential [14] results in a barrier energy of 98.3 MeV. Thus there is currently an uncertainty in the mean barrier energy of up to ±1 MeV. The effect of this uncertainty on the following analysis will be

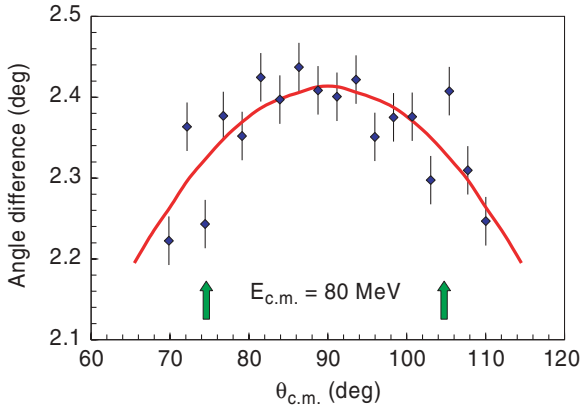

FIG. 8. (Color online) Experimental angle difference between adjacent Mott peaks in the c.m. frame compared with calculations (see text), shown as a function of the average angle of the two adjacent peaks. The arrows indicate the location of expected instrumental nonlinearities.

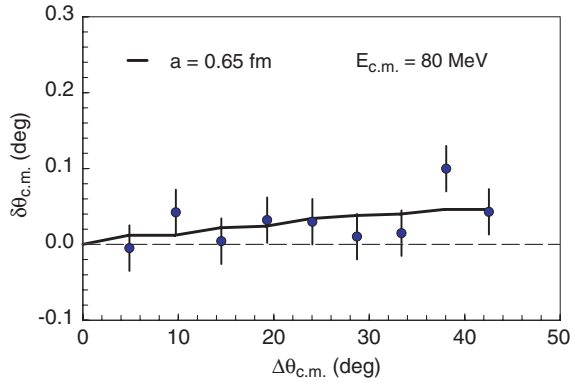

FIG. 9. (Color online) The deviation $\delta\theta$ of the measured angle separation of pairs of peaks, symmetric about 90° in the c.m. frame, from a calculation of Mott scattering with no nuclear potential and no couplings (dashed line). They are plotted as a function of the separation angle $\Delta\theta$ of the two peaks, for $E_{\text{c.m.}} = 80$ MeV. The detector was calibrated to match the trend of the calculations including couplings, which is shown by the full line (see text).

considered in Sec. IV C. Variation of the potential diffuseness parameter alone will change the energy of the fusion barrier. However, by making a small compensating change in the potential radius parameter, the fusion barrier energy was kept unchanged, independent of the diffuseness. The Woods-Saxon potential depth was kept fixed at 200 MeV.

To be consistent with the measurements, the calculations included the sum of all channels, elastic plus inelastic, and thus represent quasi-elastic differential cross sections. In the code CCFULL, the Coulomb potential includes a volume term, which changes the interaction at small separations, having a matching radius parameter of 1.1 fm. This is more realistic than a point Coulomb potential; however, even at the highest energy, changing the matching radius to 1.2 fm has no effect on the calculations.

The uncertainty in the extracted potential diffuseness will depend on the precision of the experimental peak angles. To assess this, the measured angular separation of adjacent peaks in the center-of-mass frame is shown in Fig. 8 for the $E_{\text{c.m.}} = 80$ MeV calibration reaction. The curve represents calculations with the code CCFULL, including the two-phonon coupling scheme, and a nuclear potential with diffuseness $a = 0.65$ fm. However, as expected at this subbarrier energy, the calculated Mott scattering is completely insensitive to the diffuseness. The data match the calculations well, except at the angles indicated by the arrows. These correspond to the detector angles where the effects of masking by the window support wires and local nonlinearity have their maximum effect (see Fig. 4). On the basis of the scatter of the remaining data points, the uncertainty assigned to experimental angle differences was 0.03°, corresponding to the error bars shown in the figure.

B. Extraction of diffuseness from Mott peaks

To obtain the maximum information from the experiment, while minimizing systematic uncertainties, the angle difference $\Delta\theta$ between each pair of Mott peaks symmetrically located on either side of the center-of-mass angle 90° was determined. This angle difference was referenced to that calculated with no nuclear potential and no couplings. Taking this difference resulted in the angle shift $\delta\theta$ between the measurements and simple Coulomb Mott scattering, for successive symmetric pairs of peaks. The same procedure was carried out for the CCFULL Mott scattering calculations. The results for the calibration reaction at $E_{\text{c.m.}} = 80$ MeV are shown in Fig. 9 as a function of the measured angle difference between the two paired peaks ($\Delta\theta$). The deviation of the calculation (for the two-phonon coupling scheme, and including a nuclear potential with diffuseness 0.65 fm) from the zero line indicates the (small) effect of Coulomb couplings on the Mott oscillations. There is essentially no dependence on the nuclear potential. The data at $E_{\text{c.m.}} = 80$ MeV (the true energy of 79.73 MeV after energy loss correction was used in the calculations) show good agreement with the CCFULL calculations (full line), demonstrating the excellent detector linearity and calibration. The chi-squared per degree of freedom (χ^2/n) in the comparison of the data with the calculation is 0.82, indicating that the assigned experimental angle difference uncertainty of 0.03° is not an underestimation.

The measurement at $E_{\text{c.m.}} = 95$ MeV is 4 MeV below the average fusion barrier. The dependence of the experimental $\delta\theta$ on the angle difference between the two peaks $\Delta\theta$ is shown in Fig. 10. Although the data closest to $\Delta\theta = 0°$ (coming from the two peaks closest to the 90° peak) give little information, because the angle shift due to the nuclear potential is very small, the larger angle pairs give a significant measure of the nuclear potential diffuseness. Taking the weighted average diffuseness from all angle pairs, the best-fitting diffuseness is 0.672±0.034 fm. This value gives a χ^2/n value of 0.64.

For $E_{\text{c.m.}} = 100$ MeV, close to the barrier energy, the comparison of data and calculations is shown in Fig. 11. As would be expected, the effect of the nuclear potential is larger, and thus each angle pair defines the diffuseness more

TABLE I. Best-fitting nuclear potential diffuseness parameter a for the measured energies, together with the radius parameter and χ^2/n for the best fit. The χ^2/n for the calibration energy of 160 MeV is also shown for completeness, though at this energy there is no sensitivity to the nuclear potential.

E_{lab} (MeV)	a (fm)	r_0 (fm)	χ^2/n
160	n/a	n/a	0.82
190	0.672±0.034	1.088	0.64
200	0.627±0.022	1.108	0.56
220	0.616±0.005	1.113	0.78

accurately. The weighted average of the diffuseness required for each angle pair is 0.627±0.022 fm, consistent with the result for 95 MeV, while $\chi^2/n = 0.56$.

The effect of uncertainty in the barrier energy was investigated for the 100 MeV measurement. Decreasing the nuclear potential radius parameter by 0.013 fm increased the fusion barrier energy from the standard value used, 99.0 MeV, to 100.0 MeV. For the $a = 0.65$ fm calculation, this slightly changed the calculated angle shifts $\delta\theta$ as indicated by the thick dotted line in Fig. 11, corresponding to an increase of the fitted diffuseness by ∼0.03 fm. Thus the result at this energy shows a change resulting from a reasonable variation in the barrier energy which is similar to the statistical error from the measurement. However, the importance of including couplings is illustrated by a calculation for $a = 0.65$ fm without couplings, shown by the dark (lower) dot-dashed line. This represents the change in Mott peak angles resulting only from the nuclear potential. The shift in $\delta\theta$ due to couplings alone is twice as large as found at 80 MeV, as can be seen by comparison with the full line in Fig. 9. This indicates that an analysis without including couplings will lead to different diffuseness values.

At $E_{c.m.} = 110$ MeV, which is 11 MeV above the average fusion barrier, the effect of the nuclear potential is even larger, as would be expected, and thus the measurement should give even greater sensitivity to the diffuseness. From the comparison of data and calculations, shown in Fig. 12, the

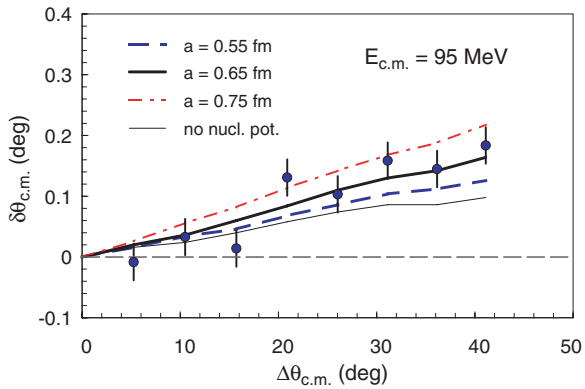

FIG. 10. (Color online) As in Fig. 9, but for $E_{c.m.} = 95$ MeV. All calculations are for the two-phonon coupling scheme, for various nuclear potential diffuseness values as indicated, and for a nuclear potential set to zero.

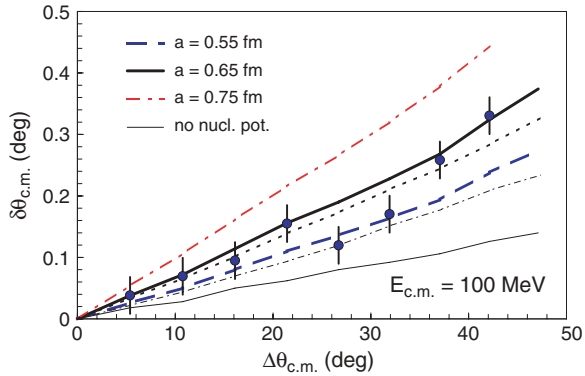

FIG. 11. (Color online) As in Fig. 10, but for a beam energy of $E_{c.m.} = 100$ MeV. The dotted line shows the small effect of varying the barrier energy by +1 MeV, for $a = 0.65$ fm, while the thin dot-dashed line shows the larger effect of a no-coupling calculation, again for $a = 0.65$.

diffuseness required to best reproduce the measurements was found to be 0.616±0.005 fm, having a $\chi^2/n = 0.78$. The results for each energy are summarized in Table I. Although there is a slight downward trend of the best-fitting diffuseness with energy, the results are consistent with a diffuseness between 0.612 and 0.620 fm ($\chi^2/n = 1.0$), independent of energy.

C. Uncertainties in the calculations

With such a small statistical uncertainty in the extracted diffuseness, resulting from the extreme sensitivity of the measurements at 110 MeV, it seems very likely that the uncertainty in the calculations would be substantially larger than those resulting from the measurements. Calculations were carried out for the 110 MeV reaction to investigate this. It might be expected that the angle shifts of the peaks could be sensitive to the couplings chosen. The effect of changing the coupling scheme was investigated for $a = 0.55$ fm. The results are shown in Fig. 12 for the one-phonon (thin dot-dashed line)

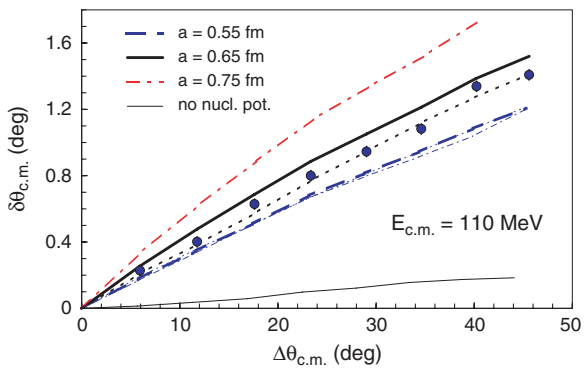

FIG. 12. (Color online) As in Fig. 10, but for $E_{c.m.} = 110$ MeV. The dotted line has the same meaning as in Fig. 10. Also shown are calculations for $a = 0.55$ fm, with one-phonon (thin dot-dashed line) and three-phonon (thin dotted line partly overlapped by the thick dashed line) coupling schemes. They hardly differ from the standard two-phonon calculation.

and three-phonon (thin dotted line) coupling schemes, which hardly differ from the standard two-phonon calculation (thick dashed line). Thus in this regard, the extracted diffuseness is rather robust. The effect of changing the coupling radius parameter was also investigated. The calculations shown up to now used the standard value of 1.2 fm, thus the accepted β_2 value of 0.1828 [15] for ^{58}Ni was used. A coupling radius parameter of 1.06 fm has been used in a number of works [16], requiring a concomitant change in the β_2 value according to the ratio of the radius parameters raised to the power of the multipolarity, giving $\beta_2 = 0.2343$. This has a relatively small effect on the calculations, increasing the diffuseness value required to fit the data by 0.02 fm (not shown in the figure). As at 100 MeV, the effect of increasing the barrier energy by 1 MeV was investigated. Calculated for $a = 0.65$ fm, the result is indicated by the thick dotted line. This reproduces the data rather well, a chi-squared analysis concluding that a 1 MeV barrier shift results in a change in extracted diffuseness of 0.04 fm, similar to the finding at 100 MeV. The latter two effects are much larger than the statistical uncertainty in the extracted diffuseness for this energy. In view of these uncertainties in the calculations, realistically, an uncertainty of perhaps ± 0.04 fm should be applied to the extracted diffuseness parameter, until a more precise barrier energy can be determined. With a more precise barrier energy, however, explicit accounting for the small effects discussed in Sec. III A may also be necessary, taking into account that the present measurement is of quasi-elastic scattering, not elastic scattering.

V. CONCLUSION

Elastic scattering of identical nuclei results in oscillatory Mott scattering. The separation of the peaks is changed by the presence of the nuclear potential. Near-barrier measurements of quasi-elastic Mott scattering of ^{58}Ni have been made, to obtain information on the tail of the nuclear potential. A coupled-channels model analysis of the shifts of the measured peak positions from those expected from a Coulomb potential alone was carried out. Measurements from 5% below to 10% above the energy of the fusion barrier were consistent with a diffuseness parameter of 0.62 fm. The main uncertainty arises from the parameters used in the coupled-channels calculations, giving an estimated uncertainty of ± 0.04 fm. This value is consistent with the nuclear potential diffuseness calculated with the double-folding model.

It is important to note that the small diffuseness value of $a = 0.62$ determined from this experiment is appropriate for the radii probed by this measurement, namely, radii outside the fusion barrier. It does not preclude a different potential behavior inside the fusion barrier [17] and/or additional physical processes beyond those included in potential models [18], which might affect the reaction process at radii inside that of the fusion barrier.

In contrast with the recently proposed analysis of quasi-elastic scattering, where deep-subbarrier measurements are optimal to minimize or even eliminate sensitivity to couplings, in the case of Mott scattering, couplings cannot be neglected at any energy. However, the results seem rather insensitive to the details of the couplings, allowing precise determination of the diffuseness parameter even at above-barrier energies, simply through matching the measured peak angles.

In other applications of Mott scattering involving heavy nuclei, such as the previous investigation [12] of a possible color van der Waals force through scattering of ^{208}Pb+^{208}Pb, the neglect of couplings to excited states may lead to incorrect conclusions, even when only considering pure elastic scattering. The version of CCFULL developed for this work allows the effects of couplings to collective vibrational states to be accounted for explicitly, and it should be used in future Mott scattering calculations where couplings are likely to be important.

This measurement of a small nuclear potential diffuseness, consistent with previous global systematics from elastic scattering [14], adds weight to the growing evidence [5,18,19] that fusion cross sections at above-barrier energies are not consistent with a description of fusion in terms of a potential model alone, with or without the inclusion of couplings. The measurement provides a diffuseness value for coupled channels calculations aiming to reproduce the recently measured fusion barrier distributions for ^{58}Ni bombarding ^{58}Ni, ^{60}Ni, and ^{64}Ni [6]. Together with accurate above-barrier [20] and deep-subbarrier cross sections [3], these results will allow a complete analysis of fusion of nickel isotopes from deep-subbarrier energies through the fusion barrier distribution to energies well above the barrier region.

ACKNOWLEDGMENTS

D.J.H. and M.D. acknowledge the financial support of Australian Research Council Discovery Grant DP0664077. The work of K.H. was supported by the Grant-in-Aid for Scientific Research, Contract No. 19740115, from the Japanese Ministry of Education, Culture, Sports, Science, and Technology.

[1] M. Beckerman, M. Salomaa, A. Sperduto, J. D. Molitoris, and A. DiRienzo, Phys. Rev. C **25**, 837 (1982).
[2] A. M. Stefanini *et al.*, Phys. Rev. Lett. **74**, 864 (1995).
[3] C. L. Jiang *et al.*, Phys. Rev. Lett. **93**, 012701 (2004).
[4] I. I. Gontchar, D. J. Hinde, M. Dasgupta, and J. O. Newton, Phys. Rev. C **69**, 024610 (2004).
[5] J. O. Newton *et al.*, Phys. Lett. **B586**, 219 (2004) ; J. O. Newton, R. D. Butt, M. Dasgupta, D. J. Hinde, I. I. Gontchar, C. R. Morton, and K. Hagino, Phys. Rev. C **70**, 024605 (2004).
[6] M. D. Rodriguez *et al.*, AIP Conf. Proc. **853**, 198 (2006).
[7] K. Hagino, T. Takehi, A. B. Balantekin, and N. Takigawa, Phys. Rev. C **71**, 044612 (2005).
[8] K. Washiyama, K. Hagino, and M. Dasgupta, Phys. Rev. C **73**, 034607 (2006).
[9] L. R. Gasques *et al.*, Phys. Rev. C (submitted).
[10] J. V. Maher *et al.*, Phys. Rev. **188**, 1665 (1969).
[11] N. F. Mott, Proc. R. Soc. London Ser. A **126**, 259 (1930).
[12] A. C. C. Villari *et al.*, Phys. Rev. Lett. **71**, 2551 (1993).

[13] K. Hagino, N. Rowley, and A. T. Kruppa, Comput. Phys. Commun. **123**, 143 (1999).
[14] O. Akyüz and A. Winther, in *Nuclear Structure and Heavy-Ion Collisions, Proceedings of the International School of Physics "Enrico Fermi", Course LXXVII, July 1979,* edited by R. A. Broglia, C. H. Dasso, and R. Ricci (North Holland, Amsterdam, 1981).
[15] S. Raman *et al*., At. Data Nucl. Data Tables **36**, 1 (1987).
[16] J. R. Leigh *et al*., Phys. Rev. C **52**, 3151 (1995).
[17] Ş. Mişicu and H. Esbensen, Phys. Rev. C **75**, 034606 (2007).
[18] M. Dasgupta, D. J. Hinde, C. Low, and J. O. Newton, AIP Conf. Proc. **853**, 21 (2006).
[19] A. Mukherjee, D. J. Hinde, M. Dasgupta, K. Hagino, J. O. Newton, and R. D. Butt, Phys. Rev. C **75**, 044608 (2007).
[20] M. D. Rodriguez *et al*. (unpublished).